


Complete substitution with modified nucleotides in self-amplifying RNA suppresses the interferon response and increases potency

Received: 15 September 2023

Accepted: 4 June 2024

Published online: 08 July 2024

 Check for updates

Joshua E. McGee^{1,2,6}, Jack R. Kirsch^{1,6}, Devin Kenney^{3,4}, Faith Cerbo^{3,4}, Elizabeth C. Chavez^{3,4}, Ting-Yu Shih⁵, Florian Douam^{3,4}, Wilson W. Wong^{1,2} & Mark W. Grinstaff^{1,5}

The use of modified nucleotides to suppress the interferon response and maintain translation of self-amplifying RNA (saRNA), which has been achieved for mRNA, has not yet succeeded. We identify modified nucleotides that, when substituted at 100% in saRNA, confer innate immune evasion and robust long-term protein expression, and when formulated as a vaccine, protect against lethal SARS-CoV-2 challenge in mice. This discovery advances saRNA therapeutics by enabling prolonged protein expression at low doses.

Substitution of chemically modified nucleotides in messenger ribonucleic acid (mRNA) enhances stability and transfection capability, and decreases immunogenicity^{1–3}, all of which enabled rapid development of vaccines against SARS-CoV-2 and propelled mRNA to the forefront of medicine^{1,4}. Native RNA activates pattern recognition receptors such as toll-like receptors and triggers type I interferon (IFN) production, resulting in translational shutoff and systemic inflammation³. Clinically approved mRNA vaccines use *N*¹-methylpseudouridine (Nm¹Ψ) to mitigate these responses and improve efficacy. Although effective, the short half-life of mRNA necessitates a large dose to be effective, which increases the risk of adverse side effects and limits accessibility.

saRNAs use an RNA-dependent RNA polymerase from an alphavirus and the corresponding conserved sequence elements at the 5' and 3' ends for replication, leading to robust and durable expression of encoded protein cargo^{5–7}. The RNA-dependent RNA polymerase also recognizes a subgenomic promoter to initiate transcription of the cargo sequence(s). saRNA can address the shortcomings of mRNA by decreasing the number of doses and the administration frequency, which will mitigate side effects^{8–10} and bolster manufacturing capacity, thus enhancing speed, reducing costs and democratizing distribution. However, early saRNA vaccine trials showed lower efficacy and

neutralizing antibody levels than mRNA vaccine trials¹¹. Recent clinical trial results revealed comparable immunogenicity of a saRNA vaccine at one-tenth of the dose of an equivalent mRNA vaccine. However, side effects were similar between the treatment groups¹².

The early and intense type I IFN response induced by saRNA detection hinders replication and antigen expression, similar to unmodified mRNA^{5,13–15}. Previous efforts to decrease the immunogenicity of saRNA focused on sequence evolution, co-expression of viral inhibitory proteins and optimization of the delivery vehicle^{16–18}. Although useful in their respective applications, all previous approaches failed to achieve a universal method of mitigating the IFN response. The best tools for such improvements are modified nucleoside triphosphates (NTPs). However, the current understanding of the field is that incorporating modified NTPs into saRNA abrogates downstream efficacy, as reported by multiple independent groups^{5,19–28}. Thus, modified nucleotides are not used.

We proposed that other modified NTPs might be compatible with saRNA and synthesized a library of saRNA constructs through *in vitro* transcription (IVT), in which all nucleotides were completely substituted with modified counterparts (Fig. 1a). To assess their functionality, we transfected these constructs, which encoded an mCherry

¹Department of Biomedical Engineering, Boston University, Boston, MA, USA. ²Biological Design Center, Boston University, Boston, MA, USA.

³Department of Virology, Immunology and Microbiology, Boston University School of Medicine, Boston, MA, USA. ⁴National Emerging Infectious Diseases Laboratories (NEIDL), Boston University, Boston, MA, USA. ⁵Department of Chemistry, Boston University, Boston, MA, USA. ⁶These authors contributed equally: Joshua E. McGee, Jack R. Kirsch. ✉ e-mail: fdouam@bu.edu; wilwong@bu.edu; mgrin@bu.edu

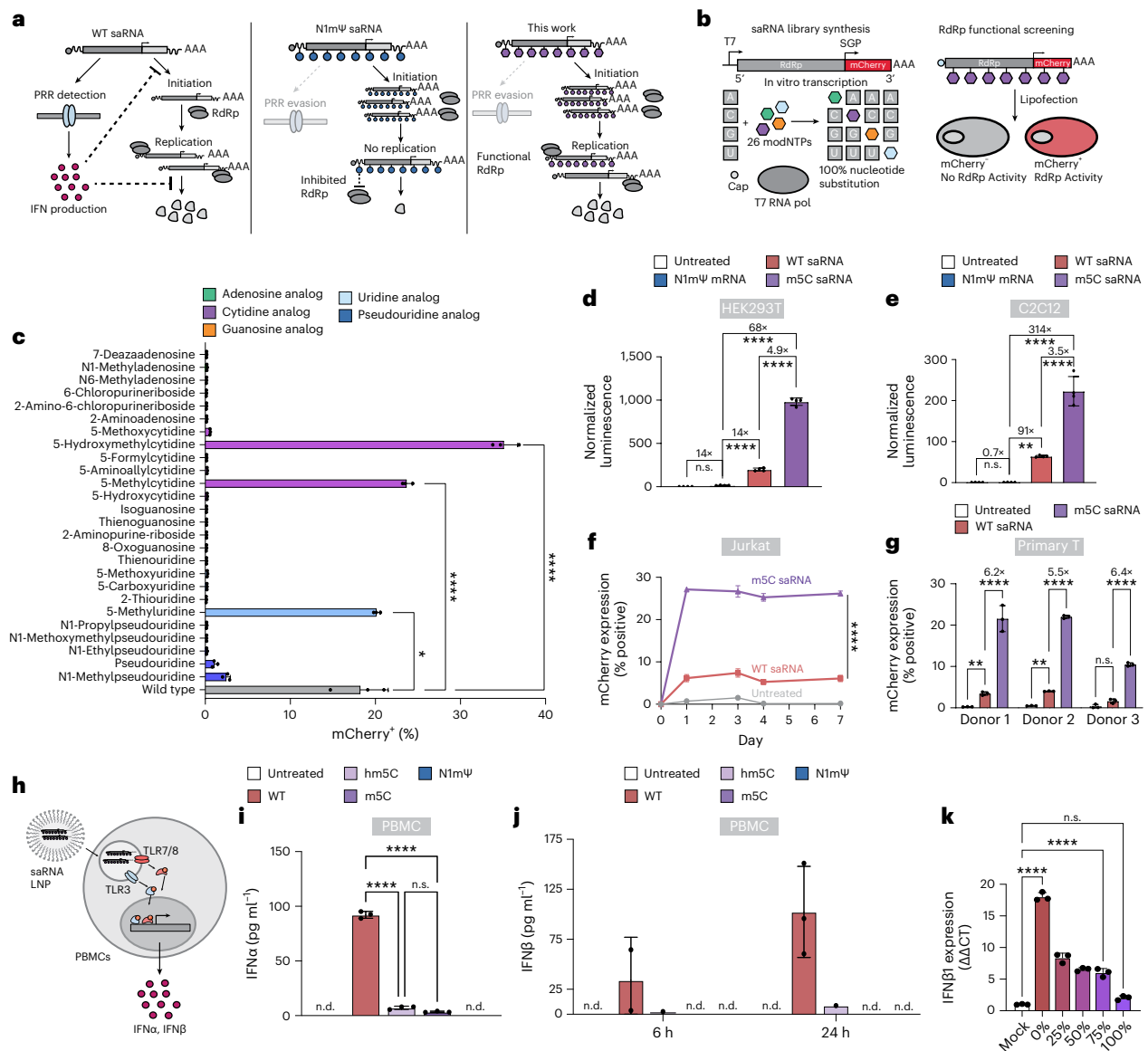


Fig. 1 | Identification of modified nucleotides compatible with saRNA and their in vitro bioactivity. **a**, Schematic illustrating the limitations of wild-type saRNA and N1mΨ-modified saRNA, and the advantages of saRNA with compatible modified NTPs. **b**, Workflow for synthesis and transfection of modified saRNA. **c**, Flow cytometry results measuring the percentage of mCherry⁺ HEK293T cells. Data are presented as mean ± s.d. (*n* = 3 biological replicates). Statistical significance was determined by one-way ANOVA with Dunnett’s multiple comparisons correction. From left to right, **P* = 3.8 × 10⁻², *****P* = 5.6 × 10⁻¹¹, *****P* = 3.0 × 10⁻¹⁵. **d**, Expression levels 24 h after LNP transfection of 10 ng of RNA encoding firefly luciferase in HEK293T cells. Luciferase signal is presented as fold change compared to mock-treated cells. Data are presented as mean ± s.d. (*n* = 4 biological replicates). Statistical significance was determined by one-way ANOVA with Tukey’s multiple comparisons correction. From top to bottom, *****P* = 2.7 × 10⁻¹⁴, *****P* = 7.3 × 10⁻¹⁴, *****P* = 4.3 × 10⁻⁷ and *n.s.* = 8.3 × 10⁻¹. **e**, Expression levels 24 h after LNP transfection of 10 ng of RNA encoding firefly luciferase in C2C12. Luciferase signal is presented as fold change compared to mock-treated cells. Data are presented as mean ± s.d. (*n* = 4 biological replicates). Statistical significance was determined by one-way ANOVA with Tukey’s multiple comparisons correction. From top to bottom, *****P* = 3.6 × 10⁻⁹, *****P* = 1.6 × 10⁻⁷, ***P* = 1.5 × 10⁻³ and *n.s.* = 9.9 × 10⁻¹. **f**, Longitudinal analysis of transfected Jurkat cells after LNP transfection with 100 ng of wild-type or m5C-modified saRNA. Data are presented as mean ± s.d. (*n* = 3 biological replicates). Statistical significance was determined by two-way ANOVA with Tukey’s multiple comparisons correction. *****P* = 4.6 × 10⁻¹⁴. **g**, Transfection efficiency 24 h after LNP transfection with 500 ng of mCherry saRNA in primary human

CD3⁺ T cells from three different donors. Data are presented as mean ± s.d. (*n* = 3 biological replicates). Statistical significance was determined by two-way ANOVA with Tukey’s multiple comparisons correction. From top to bottom, left to right, *****P* = 2.6 × 10⁻¹³, *****P* = 2.9 × 10⁻¹³, *****P* = 3.3 × 10⁻⁸, ***P* = 6.0 × 10⁻³, ***P* = 2.8 × 10⁻³ and *n.s.* = 3.5 × 10⁻¹. **h**, Assay for detecting the early IFN response from transfection of human PBMCs with unmodified or modified saRNA. **i**, IFNα (all subtypes) protein level analysis by ELISA after 6 h from a single PBMC donor treated with wild-type or modified saRNA. Data are presented as mean ± s.d. (*n* = 3 biological replicates). Statistical significance was determined by one-way ANOVA with Tukey’s multiple comparisons correction. From top to bottom, *****P* = 1.4 × 10⁻⁹, *****P* = 2.7 × 10⁻⁹ and *n.s.* = 1.4 × 10⁻¹. **j**, Analysis of IFNβ levels by ELISA from three PBMC donors after 6-h and 24-h treatment with wild-type or modified saRNA. Data are presented as mean ± s.d. (*n* = 3 biological replicates). Statistical significance was determined by one-way ANOVA with Dunnett’s multiple comparisons correction. From top to bottom, *n.s.* = 1.1 × 10⁻¹, *****P* = 2.4 × 10⁻⁷, *****P* = 1.6 × 10⁻¹³. For all statistical reporting, **P* < 0.05, ***P* < 0.01, ****P* < 0.001 and *****P* < 0.0001. CT, cycle threshold; modNTPs, modified NTPs; *n.d.*, not detected; *n.s.*, not significant; PRR, pattern recognition receptor; RdRp, RNA-dependent RNA polymerase; RNA pol, RNA polymerase; SGP, subgenomic promoter; TLR3, toll-like receptor 3; TLR7/8, toll-like receptors 7 and 8; WT, wild-type.

reporter, into HEK293T cells by cationic lipofection (Fig. 1b). Three modified NTPs afford significantly elevated transfection efficiencies when incorporated into saRNA. Constructs with complete substitution of 5-hydroxymethylcytidine (hm5C), 5-methylcytidine (m5C) or 5-methyluridine (m5U) exhibit transfection efficiencies 14-fold, 10-fold and 8-fold higher than the N1m Ψ -modified construct, respectively, as revealed by flow cytometry analysis (Fig. 1c and Supplementary Fig. 1a,b) and live-cell microscopy (Supplementary Fig. 1c). The transfection efficiencies of the hm5C and m5C constructs are also significantly greater than the wild-type (WT) saRNA. Substitution with the identified modified NTPs results in functional constructs synthesized with a Cap-0 or Cap-1 structure (Supplementary Fig. 1d).

Next, we investigated wild-type saRNA, m5C saRNA and N1m Ψ mRNA, all of which encode a luciferase reporter construct, and loaded these into lipid nanoparticles (LNPs). We transfected HEK293T and C2C12 cells with 10 ng of RNA. Notably, the m5C saRNA exhibits a 4.9-fold higher protein expression than the wild-type saRNA, corresponding to a 68-fold higher expression than the N1m Ψ mRNA in HEK293T cells (Fig. 1d). In fact, significant expression occurs at doses as low as 1 ng (Supplementary Fig. 2a). In C2C12 cells, the m5C saRNA affords a 3.5-fold higher protein expression, resulting in a 314-fold higher expression compared to the N1m Ψ mRNA (Fig. 1e). In LNP-transfected Jurkat cells, 25 or 250 ng of m5C saRNA results in a 17.8-fold or an 8.2-fold improvement in protein expression, respectively, compared to wild-type saRNA (Supplementary Fig. 2b–d). The protein expression profile is similar for the luciferase constructs at 250 ng (Supplementary Fig. 2e). In a time-course study, the m5C saRNA leads to durable expression over 7 days in LNP-transfected Jurkat cells (Fig. 1f and Supplementary Fig. 2f). Denaturing gel electrophoresis reveals comparable transcript length and quality for modified saRNAs encoding mCherry (Supplementary Fig. 3a). Furthermore, encapsulation of the RNA is similar between modified constructs (>90% encapsulation efficiency; Supplementary Fig. 3b). By contrast, the N1m Ψ saRNA does not produce detectable levels of mCherry expression after LNP transfection or electroporation (Supplementary Fig. 3c,d).

We then treated CD3⁺ T cells, derived from three different human donors, with wild-type saRNA-loaded or m5C saRNA-loaded LNPs. Transfection efficiency increases five- to sixfold with m5C saRNA-loaded LNPs compared to the wild-type saRNA-loaded LNPs (Fig. 1g and Supplementary Fig. 4a,b). The mCherry reporter expression is present for at least 5 days (Supplementary Fig. 4b).

To investigate the contribution of double-stranded RNA (dsRNA) impurities on transfection, we performed additional studies with dsRNA-depleted RNA²⁹. We synthesized N1m Ψ mRNA, wild-type saRNA, hm5C saRNA and m5C saRNA encoding firefly luciferase by IVT followed by cellulose chromatography³⁰. All RNAs show minimal degradation (Supplementary Fig. 5a). Dot blotting reveals minimal dsRNA in N1m Ψ mRNA, even before cellulose purification. By contrast, wild-type saRNA contain dsRNA impurities, approximately fivefold and threefold higher than hm5C and m5C saRNAs, respectively (Supplementary Fig. 5b). After two rounds of cellulose chromatography, dsRNA impurities are at or below the detection limit for all RNAs. We transfected the purified RNAs into Jurkat cells. At 10 ng, purified hm5C and m5C saRNAs affords 146-fold and 75-fold greater protein production than wild-type saRNA, and 36-fold and 18-fold greater protein production than N1m Ψ mRNA, respectively (Supplementary Fig. 5c). Similar trends in protein production are present at 100 ng, with hm5C and m5C saRNAs outperforming wild-type saRNA and N1m Ψ mRNA. In primary human foreskin fibroblasts, N1m Ψ mRNA exhibits a linear dose response, whereas saRNA shows a nonlinear dose response (Supplementary Fig. 5d). At the lowest dose, hm5C and m5C saRNAs produces significantly greater protein levels than N1m Ψ mRNA (112-fold and 93-fold, respectively) and wild-type saRNA (4.4-fold and 3.6-fold, respectively). At the highest dose, the differences in protein expression is not significantly different between the treatment groups.

To characterize the IFN response caused by wild-type or modified saRNA, we cultured human peripheral blood mononuclear cells (PBMCs) from three distinct donors with LNPs loaded with saRNA (Fig. 1h). saRNA treatment, as revealed by gene expression analysis, induces a significant increase in the expression of early IFN-related genes, namely, IFN α 1, IFN α 2 and IFN β 1, after 6 h (Supplementary Fig. 6a–c). However, when hm5C or m5C is incorporated, the expression levels of IFN α 1 and IFN β 1 reduce by 8.5-fold and 3-fold, respectively. The analysis of IFN α subtypes in culture media from a single donor (Fig. 1i) is consistent with the gene expression analysis. A longitudinal analysis of human IFN β in culture media reveals that the incorporation of hm5C, m5C, m5U and N1m Ψ effectively suppresses IFN β expression. Across all donors, no detectable expression of IFN β is present after m5C and N1m Ψ saRNA treatment, and only one donor exhibits detectable levels of IFN β after hm5C saRNA treatment (Fig. 1j). To determine the effect of partial versus complete m5C substitution on the IFN response, we cultured PBMCs with saRNA synthesized with 0%, 25%, 50%, 75% and 100% m5C substitution and measured the IFN β 1 expression. IFN β 1 expression decreases with increasing concentrations of m5C (Fig. 1k), and at 100% substitution, IFN β 1 expression is similar to that of the untreated control cells.

Next, we evaluated the protein expression levels and kinetics of wild-type saRNA, m5C saRNA and N1m Ψ mRNA in vivo using bioluminescent imaging. We administered intramuscular (i.m.) injections of PBS or 2.5 μ g of N1m Ψ mRNA, wild-type saRNA or m5C saRNA encoding firefly luciferase to C57BL/6 mice ($n = 5$ per group). The group that received N1m Ψ mRNA attains peak protein expression at 24 h, and then the signal rapidly decreases (Fig. 2a,b). By contrast, the groups treated with wild-type or m5C saRNA show a consistent increase in the signal and, 7 days after the initial injection, reached peak protein expression that is four times greater than the N1m Ψ mRNA group (Fig. 2b and Supplementary Fig. 7a). We observed no significant differences in expression levels or duration of expression between the groups that received wild-type or m5C saRNA. However, the systemic level of IFN α 1 6 h after injection is 2.2-fold lower in the group treated with m5C RNA (Supplementary Fig. 7b). Notably, the groups that were administered wild-type or m5C saRNA both display significantly prolonged protein expression throughout the 28-day study duration (Fig. 2b).

We then generated nonreplicating mRNA (spike mRNA) and saRNA (spike saRNA) encoding a K986P-stabilized and V987P-stabilized spike protein of SARS-CoV-2 derived from the Wuhan-1 (WA-1) strain (Fig. 2c). We assembled the constructs by IVT and then transfected these LNP-encapsulated RNAs into HEK293T and C2C12 cells using LNPs. In HEK293T cells, hm5C, m5C and m5U saRNAs exhibit approximately twice the protein expression compared to wild-type saRNA (Fig. 2d). Consistent with previous findings, N1m Ψ saRNA results in suppressed protein expression. In C2C12 cells, both hm5C and m5C saRNA afford a twofold higher protein expression than wild-type saRNA and approximately an 8-fold higher protein expression than N1m Ψ mRNA (Fig. 2e,f and Supplementary Fig. 8a; see Supplementary Fig. 8b for confirmation with ELISA). Notably, the m5U modification does not result in protein expression in C2C12 cells. We performed similar in vitro experiments to evaluate the expression of the influenza hemagglutinin antigen, and the expression profile is consistent with our previous experiments (Supplementary Fig. 8c,d).

Motivated by the increased antigen expression in vitro and the durable expression in vivo, we evaluated the effectiveness of the m5C saRNA vaccine against SARS-CoV-2 infection. In healthy C57BL/6 mice, we administered intramuscular (i.m.) injections of 10 ng, 100 ng or 1,000 ng of wild-type or m5C saRNA, which encoded the spike protein, and then boosted at 21 days post initial vaccination (Fig. 2g). Additional cohorts in the study received 10 ng or 1,000 ng of N1m Ψ mRNA to evaluate comparative performance at a low and high dose, respectively, or PBS. The intermediate dose of 100 ng N1m Ψ mRNA produces a weak antibody response in previous reports³¹. To assess the

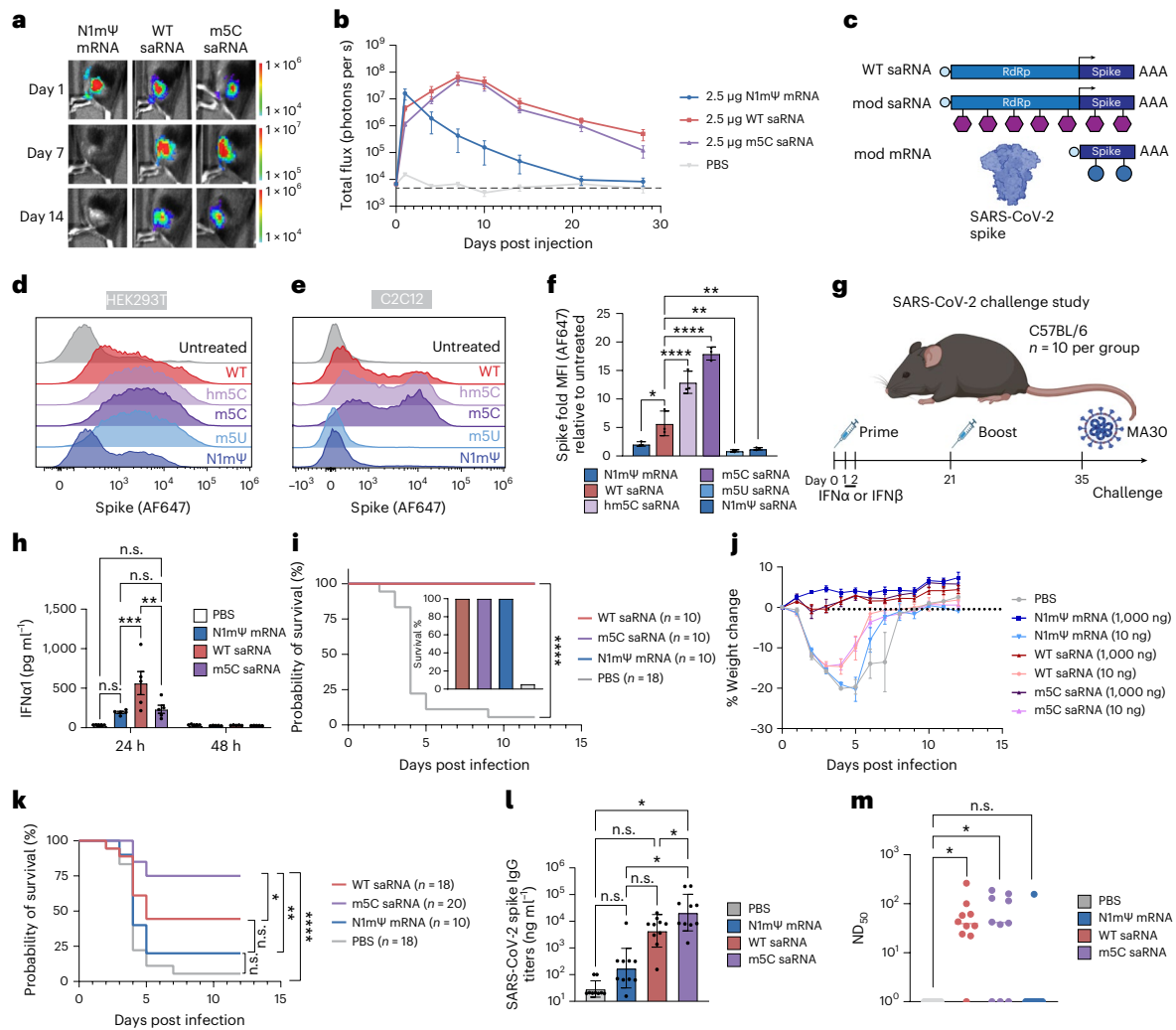


Fig. 2 | Development and characterization of a fully modified saRNA vaccine against SARS-CoV-2. **a**, Bioluminescent images of mice at different time points after i.m. injection of LNPs containing 2.5 μg of luciferase encoding N1mΨ mRNA (left), wild-type saRNA (middle) or m5C saRNA (right). Scale bar indicates radiance. **b**, Total flux (photons per second) from bioluminescent imaging of mice administered LNPs containing 2.5 μg of luciferase encoding N1mΨ mRNA, wild-type saRNA or m5C saRNA by i.m. injection ($n = 5$ biological replicates). Dashed line indicates average signal for the PBS group over the duration of the study. Data are presented as mean \pm s.e.m. **c**, Schematic illustrating RNA formats for expression of the SARS-CoV-2 spike protein evaluated in this study. **d**, Expression of spike protein detected by flow cytometry 24 h after LNP transfection with 100 ng of RNA in HEK293T cells (representative of $n = 3$ biological replicates). y-axis values are normalized to mode. **e**, Expression of spike protein detected by flow cytometry 24 h after LNP transfection with 100 ng of RNA in C2C12 cells (representative of $n = 3$ biological replicates). y-axis values are normalized to mode. **f**, Median fluorescence intensity (MFI) of anti-spike Alexa Fluor 647 (AF647) stained C2C12 cells. MFI is relative to untreated cells stained with anti-spike AF647. Data are presented as mean \pm s.d. ($n = 3$ biological replicates). Statistical significance was determined by one-way ANOVA with Dunnett's multiple comparisons correction. From top to bottom, $^{**}P = 4.9 \times 10^{-3}$, $^{**}P = 2.8 \times 10^{-3}$, $^{****}P = 3.1 \times 10^{-7}$, $^{****}P = 7.9 \times 10^{-5}$ and $^{*}P = 2.0 \times 10^{-2}$. **g**, Study design for the SARS-CoV-2 challenge study in C57BL/6 mice. Black line indicates analysis of samples collected on days 1 and 2. **h**, IFN α 1 protein levels measured in serum collected 24 h or 48 h after initial vaccination with 1,000 ng of RNA in LNPs. Data are presented as mean \pm s.e.m. ($n = 5$ biological replicates). Statistical significance was determined by two-way ANOVA with Sidak's multiple comparisons correction. From top to bottom, n.s. = 6.0×10^{-2} , n.s. = 9.9×10^{-1} , $^{**}P = 1.0 \times 10^{-3}$, $^{***}P = 2.3 \times 10^{-4}$ and n.s. = 1.8×10^{-1} . **i**, Survival of mice vaccinated with 1,000 ng after lethal challenge with MA30 virus. Wild-type saRNA, $n = 10$ biological replicates; m5C saRNA, $n = 10$ biological replicates;

N1mΨ mRNA, $n = 10$ biological replicates; PBS, $n = 18$ biological replicates. Statistical significance was determined by the Mantel–Cox log-rank test. $^{****}P = 2.7 \times 10^{-6}$. **j**, Longitudinal weight change of mice after lethal challenge. Data are presented as mean \pm s.e.m. 1,000 ng N1mΨ mRNA, $n = 10$ biological replicates; 10 ng N1mΨ mRNA, $n = 10$ biological replicates; 1,000 ng wild-type saRNA, $n = 10$ biological replicates; 10 ng wild-type saRNA, $n = 18$ biological replicates; 1,000 ng m5C saRNA, $n = 10$ biological replicates; m5C saRNA, $n = 20$ biological replicates. **k**, Survival of mice vaccinated with 10 ng after lethal challenge with MA30 virus. Wild-type saRNA, $n = 18$ biological replicates; m5C saRNA, $n = 20$ biological replicates; N1mΨ mRNA, $n = 10$ biological replicates; PBS, $n = 18$ biological replicates. Statistical significance was determined by the Mantel–Cox log-rank test. From left to right, n.s. = 2.6×10^{-1} , n.s. = 2.4×10^{-1} , $^{*}P = 4.4 \times 10^{-2}$, $^{**}P = 1.9 \times 10^{-3}$ and $^{****}P = 2.9 \times 10^{-6}$. **l**, SARS-CoV-2 spike protein-reactive IgG titers measured from the serum of animals vaccinated with 10 ng of RNA collected on day 35. N1mΨ mRNA, $n = 10$ biological replicates; wild-type saRNA, $n = 10$ biological replicates; m5C saRNA, $n = 10$ biological replicates; PBS, $n = 9$ biological replicates. Data are presented as geometric mean \pm geometric s.d. Statistical significance was determined by one-way ANOVA with Tukey's multiple comparisons correction. From top to bottom, left to right, $^{*}P = 2.2 \times 10^{-2}$, n.s. = 9.8×10^{-1} , $^{*}P = 4.8 \times 10^{-2}$, $^{*}P = 2.1 \times 10^{-2}$, n.s. = 9.8×10^{-1} and n.s. = 9.9×10^{-1} . **m**, Neutralization titer (dilution resulting in 50% infection inhibition) values measured from the serum of animals vaccinated with 10 ng of RNA. Horizontal lines indicate the median values. PBS, $n = 9$ biological replicates; N1mΨ mRNA, $n = 10$ biological replicates; wild-type saRNA, $n = 10$ biological replicates; m5C saRNA, $n = 10$ biological replicates. Statistical significance was determined by one-way ANOVA with Dunnett's multiple comparisons correction. From top to bottom, n.s. = 8.7×10^{-1} , $^{*}P = 2.4 \times 10^{-2}$ and $^{*}P = 4.6 \times 10^{-2}$. For all statistical reporting, $^{*}P < 0.05$, $^{**}P < 0.01$, $^{***}P < 0.001$ and $^{****}P < 0.0001$. ND $_{50}$, 50% neutralizing dose.

early IFN response in mice, serum was collected from mice vaccinated with the 1,000-ng dose at 24 h and 48 h. Significantly reduced levels of serum IFN α 1 are present in mice that received N1m Ψ mRNA or m5C saRNA compared to mice that were administered wild-type saRNA. By 48 h post vaccination, IFN α 1 is no longer detectable in the serum of any of the mice (Fig. 2h). Across all samples, IFN β is not detectable at 24 h or 48 h (Supplementary Fig. 9a). On day 35, we intranasally infected the mice with a lethal dose of 1×10^5 plaque-forming units of mouse-adapted SARS-CoV-2 (MA30)³². The mice vaccinated with 1,000 ng of wild-type saRNA, m5C saRNA or N1m Ψ mRNA show 100% survival and minimal weight loss (Fig. 2i,j). Similarly, mice vaccinated with 100 ng of wild-type or m5C saRNA survive, with an average weight loss of 5% (Supplementary Fig. 9b,c). However, the survival rates are 20% and 45% for mice receiving the 10-ng dose of N1m Ψ mRNA or wild-type saRNA, respectively, and the mice lost significant weight (Fig. 2j,k). By contrast, survival is significantly higher in mice vaccinated with the 10-ng dose of m5C saRNA (75% survival) upon viral challenge compared to animals treated with N1m Ψ mRNA, wild-type saRNA or PBS (Fig. 2k).

To investigate the observed differences in protection among groups, we measured SARS-CoV-2 spike protein-reactive immunoglobulin G (IgG) titers in serum collected from the same cohort of mice on day 35. Titers ranged from 10^6 to 10^7 ng ml⁻¹, with no significant differences between the 1,000-ng wild-type saRNA, m5C saRNA and N1m Ψ mRNA treatment groups (Supplementary Fig. 9d). For mice vaccinated with 100 ng of wild-type saRNA or m5C saRNA, titers vary between 10^5 and 10^6 ng ml⁻¹, showing no significant difference between the two groups (Supplementary Fig. 9e). In contrast, at the 10-ng dose, animals vaccinated with m5C saRNA display significantly elevated titers, with a 5-fold higher titer than wild-type saRNA vaccinated animals and a 121-fold higher titer N1m Ψ mRNA-vaccinated animals (Fig. 2l).

To determine whether survival in mice vaccinated with 5mC saRNA is associated with increased serum neutralizing titers, we evaluated the neutralizing activity of serum samples from mice vaccinated with 10 ng of wild-type saRNA, m5C saRNA or N1m Ψ mRNA against infectious SARS-CoV-2 WA-1. Sera from mice that were administered vehicle or 10 ng of N1m Ψ mRNA do not significantly neutralize WA-1, whereas serum samples from mice vaccinated with 10 ng of wild-type or 5mC saRNA elicit similar neutralizing activity (Fig. 2m). No association between survival and neutralizing antibody levels is observed in mice vaccinated with wild-type saRNA or m5C saRNA (Supplementary Fig. 9f).

saRNA promises lower-dose vaccines and off-the-shelf, in situ, long-lasting and non-integrating cell and gene therapies. Unfortunately, the clinical reality thus far paints a less encouraging picture⁶, although the recent regulatory approval of a wild-type saRNA in Japan bodes well for the future of saRNA technologies^{33,34}. Preclinical and clinical data confirm that the early and intense IFN response inhibits antigen expression and induces inflammation^{5,13,14,35}. A mechanism to effectively evade the early IFN response, improve saRNA transfection and reduce reactogenicity would unlock the true potential of the platform.

Anti-spike antibody titers are a potential correlate of protection upon m5C saRNA vaccination (Fig. 2l). Serum neutralizing antibody titers are similar between wild-type and m5C saRNA-treated mice, even though protection from fatal infection is not. Serum neutralizing activity is one of many correlates of protection, and although SARS-CoV-2 variants have been associated with escape of vaccine-induced neutralizing antibodies^{36–41}, clinical protection is maintained through vaccine-induced T cell responses and Fc effector functions^{42–46}. Our findings suggest that the correlates of protection associated with low-dose m5C saRNA vaccination extend beyond neutralizing humoral responses. This point is further strengthened by the lack of positive correlation between survival and neutralizing titers in mice vaccinated with wild-type or m5C saRNA (Supplementary Fig. 9f).

Future work will evaluate the contribution of Fc effector functions and T cell responses.

Recently, a study reported that 5% m5C-modified saRNA affords a functional construct as a SARS-CoV-2 booster in a phase I human safety study⁴⁷. Healthy participants vaccinated with LNPs containing 1, 3, 7.5, or 15 μ g of 5% m5C saRNA had ~3-fold higher IgG titers at day 28. No comparator arms that included modified mRNA or wild-type saRNA were reported. This work highlights the potential clinical utility of modified saRNA through positive human safety studies. Another study⁴⁸ demonstrated that saRNA, when fully substituted with m5C, exhibits a notable decrease in the innate immune response compared to wild-type saRNA in vitro. These results further support exploration of m5C-modified saRNA. The next logical step in development is to use clinical-grade saRNA to evaluate safety and efficacy in non-human primate and human studies.

Other emerging RNA formats, notably circular RNA, may benefit from similar endeavors to screen for compatible modified nucleotides^{49–52} and may shed light on the compatibility and interactions of modified nucleotides with diverse RNA structures. Similarly, exploring the effects of modified nucleotides in the broader family of alphaviruses will also be key to further unlocking the potential of modified saRNA. This discovery enhances the potency of RNA vaccines and broadens the utility of saRNA.

Online content

Any methods, additional references, Nature Portfolio reporting summaries, source data, extended data, supplementary information, acknowledgements, peer review information; details of author contributions and competing interests; and statements of data and code availability are available at <https://doi.org/10.1038/s41587-024-02306-z>.

References

- Kariko, K. et al. Incorporation of pseudouridine into mRNA yields superior nonimmunogenic vector with increased translational capacity and biological stability. *Mol. Ther.* **16**, 1833–1840 (2008).
- Kormann, M. S. et al. Expression of therapeutic proteins after delivery of chemically modified mRNA in mice. *Nat. Biotechnol.* **29**, 154–157 (2011).
- Anderson, B. R. et al. Incorporation of pseudouridine into mRNA enhances translation by diminishing PKR activation. *Nucleic Acids Res.* **38**, 5884–5892 (2010).
- Kariko, K., Buckstein, M., Ni, H. & Weissman, D. Suppression of RNA recognition by toll-like receptors: the impact of nucleoside modification and the evolutionary origin of RNA. *Immunity* **23**, 165–175 (2005).
- Minnaert, A. K. et al. Strategies for controlling the innate immune activity of conventional and self-amplifying mRNA therapeutics: getting the message across. *Adv. Drug Deliv. Rev.* **176**, 113900 (2021).
- Geall, A. J., Kis, Z. & Ulmer, J. B. Vaccines on demand, part II: future reality. *Expert Opin. Drug Discov.* **18**, 119–127 (2023).
- Bloom, K., van den Berg, F. & Arbuthnot, P. Self-amplifying RNA vaccines for infectious diseases. *Gene Ther.* **28**, 117–129 (2021).
- Trougakos, I. P. et al. Adverse effects of COVID-19 mRNA vaccines: the spike hypothesis. *Trends Mol. Med.* **28**, 542–554 (2022).
- Ndeupen, S. et al. The mRNA-LNP platform's lipid nanoparticle component used in preclinical vaccine studies is highly inflammatory. *iScience* **24**, 103479 (2021).
- Ju, Y. et al. Impact of anti-PEG antibodies induced by SARS-CoV-2 mRNA vaccines. *Nat. Rev. Immunol.* **23**, 135–136 (2023).
- Low, J. G. et al. A phase I/II randomized, double-blinded, placebo-controlled trial of a self-amplifying Covid-19 mRNA vaccine. *NPJ Vaccines* **7**, 161 (2022).

12. Akahata, W. et al. Safety and immunogenicity of SARS-CoV-2 self-amplifying RNA vaccine expressing an anchored RBD: a randomized, observer-blind phase 1 study. *Cell Rep. Med.* **4**, 101134 (2023).
13. Zhong, Z. et al. Corticosteroids and cellulose purification improve, respectively, the in vivo translation and vaccination efficacy of sa-mRNAs. *Mol. Ther.* **29**, 1370–1381 (2021).
14. Pepini, T. et al. Induction of an IFN-mediated antiviral response by a self-amplifying RNA vaccine: implications for vaccine design. *J. Immunol.* **198**, 4012–4024 (2017).
15. Huysmans, H. et al. Expression kinetics and innate immune response after electroporation and LNP-mediated delivery of a self-amplifying mRNA in the skin. *Mol. Ther. Nucleic Acids* **17**, 867–878 (2019).
16. Li, Y. et al. In vitro evolution of enhanced RNA replicons for immunotherapy. *Sci. Rep.* **9**, 6932 (2019).
17. Blakney, A. K. et al. Innate inhibiting proteins enhance expression and immunogenicity of self-amplifying RNA. *Mol. Ther.* **29**, 1174–1185 (2021).
18. Kimura, T. et al. A localizing nanocarrier formulation enables multi-target immune responses to multivalent replicating RNA with limited systemic inflammation. *Mol. Ther.* **31**, 2360–2375 (2023).
19. Kairuz, D., Samudh, N., Ely, A., Arbuthnot, P. & Bloom, K. Advancing mRNA technologies for therapies and vaccines: an African context. *Front. Immunol.* **13**, 1018961 (2022).
20. Voigt, E. A. et al. A self-amplifying RNA vaccine against COVID-19 with long-term room-temperature stability. *NPJ Vaccines* **7**, 136 (2022).
21. Beissert, T. et al. A trans-amplifying RNA vaccine strategy for induction of potent protective immunity. *Mol. Ther.* **28**, 119–128 (2020).
22. Geall, A., Hekele, A. & Mandl, C. RNA containing modified nucleotides and use thereof in vaccines. WIPO publication no. WO2011/005799A3 (2010); <https://patentscope.wipo.int/search/en/detail.jsf?docId=WO2011005799>
23. Erasmus, J. H. et al. Intramuscular delivery of replicon RNA encoding ZIKV-117 human monoclonal antibody protects against Zika virus infection. *Mol. Ther. Methods Clin. Dev.* **18**, 402–414 (2020).
24. Pollock, K. M. et al. Safety and immunogenicity of a self-amplifying RNA vaccine against COVID-19: COVAC1, a phase I, dose-ranging trial. *EClinicalMedicine* **44**, 101262 (2022).
25. Blakney, A. K. et al. Effects of cationic adjuvant formulation particle type, fluidity and immunomodulators on delivery and immunogenicity of saRNA. *J. Control. Release* **304**, 65–74 (2019).
26. Papukashvili, D. et al. Self-amplifying RNA approach for protein replacement therapy. *Int. J. Mol. Sci.* **23**, 12884 (2022).
27. Kairuz, D., Samudh, N., Ely, A., Arbuthnot, P. & Bloom, K. Production, characterization, and assessment of permanently cationic and ionizable lipid nanoparticles for use in the delivery of self-amplifying RNA vaccines. *Pharmaceutics* **15**, 1173 (2023).
28. Deering, R. P., Kommareddy, S., Ulmer, J. B., Brito, L. A. & Geall, A. J. Nucleic acid vaccines: prospects for non-viral delivery of mRNA vaccines. *Expert Opin. Drug Deliv.* **11**, 885–899 (2014).
29. Kariko, K., Muramatsu, H., Ludwig, J. & Weissman, D. Generating the optimal mRNA for therapy: HPLC purification eliminates immune activation and improves translation of nucleoside-modified, protein-encoding mRNA. *Nucleic Acids Res.* **39**, e142 (2011).
30. Baiersdorfer, M. et al. A facile method for the removal of dsRNA contaminant from in vitro-transcribed mRNA. *Mol. Ther. Nucleic Acids* **15**, 26–35 (2019).
31. de Alwis, R. et al. A single dose of self-transcribing and replicating RNA-based SARS-CoV-2 vaccine produces protective adaptive immunity in mice. *Mol. Ther.* **29**, 1970–1983 (2021).
32. Dinno, K. H. 3rd et al. A mouse-adapted model of SARS-CoV-2 to test COVID-19 countermeasures. *Nature* **586**, 560–566 (2020).
33. CSL. Japan's Ministry of Health, Labour and Welfare approves CSL and Arcturus Therapeutics' ARCT-154, the first self-amplifying mRNA vaccine approved for COVID in adults. <https://newsroom.csl.com/2023-11-28-Japans-Ministry-of-Health,-Labour-and-Welfare-Approves-CSL-and-Arcturus-Therapeutics-ARCT-154,-the-first-Self-Amplifying-mRNA-vaccine-approved-for-COVID-in-adults> (27 November 2023).
34. Dolgin, E. Self-copying RNA vaccine wins first full approval: what's next? *Nature* **624**, 236–237 (2023).
35. Zhong, Z. et al. Immunogenicity and protection efficacy of a naked self-replicating mRNA-based Zika virus vaccine. *Vaccines* **7**, 96 (2019).
36. Kurhade, C. et al. Low neutralization of SARS-CoV-2 Omicron BA.2.75.2, BQ.1.1 and XBB.1 by parental mRNA vaccine or a BA.5 bivalent booster. *Nat. Med.* **29**, 344–347 (2023).
37. Miller, J. et al. Substantial neutralization escape by SARS-CoV-2 Omicron variants BQ.1.1 and XBB.1. *N. Engl. J. Med.* **388**, 662–664 (2023).
38. Arora, P. et al. Neutralisation sensitivity of the SARS-CoV-2 XBB.1 lineage. *Lancet Infect. Dis.* **23**, 147–148 (2023).
39. Hachmann, N. P., Miller, J., Collier, A. Y. & Barouch, D. H. Neutralization escape by SARS-CoV-2 Omicron subvariant BA.4.6. *N. Engl. J. Med.* **387**, 1904–1906 (2022).
40. Andrews, N. et al. Covid-19 vaccine effectiveness against the Omicron (B.1.1.529) variant. *N. Engl. J. Med.* **386**, 1532–1546 (2022).
41. Cele, S. et al. Omicron extensively but incompletely escapes Pfizer BNT162b2 neutralization. *Nature* **602**, 654–656 (2022).
42. Gao, Y. et al. Ancestral SARS-CoV-2-specific T cells cross-recognize the Omicron variant. *Nat. Med.* **28**, 472–476 (2022).
43. GeurtsvanKessel, C. H. et al. Divergent SARS-CoV-2 Omicron-reactive T and B cell responses in COVID-19 vaccine recipients. *Sci. Immunol.* **7**, eabo2202 (2022).
44. Addetia, A. et al. Neutralization, effector function and immune imprinting of Omicron variants. *Nature* **621**, 592–601 (2023).
45. Keeton, R. et al. T cell responses to SARS-CoV-2 spike cross-recognize Omicron. *Nature* **603**, 488–492 (2022).
46. Kaplonek, P. et al. mRNA-1273 vaccine-induced antibodies maintain Fc effector functions across SARS-CoV-2 variants of concern. *Immunity* **55**, 355–365.e4 (2022).
47. Aboshi, M. et al. Safety and immunogenicity of VLPCOV-02, a SARS-CoV-2 self-amplifying RNA vaccine with a modified base, 5-methylcytosine. *iScience* **27**, 108964 (2024).
48. Komori, M. et al. Incorporation of 5 methylcytidine alleviates innate immune response to self-amplifying RNA vaccine. Preprint at *bioRxiv* <https://doi.org/10.1101/2023.11.01.565056> (2023).
49. Chen, C. K. et al. Structured elements drive extensive circular RNA translation. *Mol. Cell* **81**, 4300–4318.e13 (2021).
50. Chen, R. et al. Engineering circular RNA for enhanced protein production. *Nat. Biotechnol.* **41**, 262–272 (2023).
51. Kameda, S., Ohno, H. & Saito, H. Synthetic circular RNA switches and circuits that control protein expression in mammalian cells. *Nucleic Acids Res.* **51**, e24 (2023).
52. Wesselhoeft, R. A., Kowalski, P. S. & Anderson, D. G. Engineering circular RNA for potent and stable translation in eukaryotic cells. *Nat. Commun.* **9**, 2629 (2018).

Publisher's note Springer Nature remains neutral with regard to jurisdictional claims in published maps and institutional affiliations.

Springer Nature or its licensor (e.g. a society or other partner) holds exclusive rights to this article under a publishing agreement with the author(s) or other rightsholder(s); author

self-archiving of the accepted manuscript version of this article is solely governed by the terms of such publishing agreement and applicable law.

© The Author(s), under exclusive licence to Springer Nature America, Inc. 2024

Methods

Template design and synthesis

All mRNA and saRNA templates took the form of linearized plasmid DNA. All saRNA templates were generated from a plasmid encoding nonstructural proteins 1–4 of the Venezuelan equine encephalitis virus (VEEV) using either a CleanCap AU (TriLink BioTechnologies)-compatible T7 promoter (promoter sequence, TAATACGACTCACTATAAT) or a guanosine-5'-triphosphate (GTP)-compatible and anti-reverse cap analog (ARCA)-compatible T7 promoter (promoter sequence, TAATACGACTCACTATAGGAT). Sequences from VEEV were derived from T7-VEE-GFP⁵³, which was deposited by S. Dowdy (Addgene plasmid no. 58977)⁵⁴. Reporter plasmids were generated by inserting the coding sequences for mCherry or firefly luciferase between 5' and 3' UTR sequences derived from human beta-globin. The National Center for Biotechnology Information (NCBI) reference sequence for the influenza A hemagglutinin (Influenza A virus (A/California/07/2009(H1N1))) is available at [YP_009118626.1](https://www.ncbi.nlm.nih.gov/nuclom/YP_009118626.1), and the NCBI reference sequence for the SARS-CoV-2 spike protein with K986P-stabilizing and V987P-stabilizing mutations (Wuhan-Hu-1) is available at [YP_009724390.1](https://www.ncbi.nlm.nih.gov/nuclom/YP_009724390.1). Plasmids were cloned in DH5α *Escherichia coli*, purified using a ZymoPURE II Plasmid Midiprep Kit (Zymo Research), linearized with MluI-HF for 3 h at 37 °C and purified again using a QIAquick PCR Purification Kit (Qiagen).

RNA synthesis

mRNA and saRNA were synthesized using the MEGAscript T7 Transcription Kit (Thermo Fisher Scientific) with 1 μg template and co-transcriptional capping through CleanCap AU (TriLink BioTechnologies). For IVT with ARCA, final concentrations of 12 mM ARCA and 4 mM GTP were used. For ARCA experiments in which a GTP analog was used, the modified NTP was completely substituted to a final concentration of 4 mM. The modified NTPs in all CleanCap AU IVT reactions were prepared according to the manufacturer's protocol. IVT was performed for 3 h at 37 °C, followed by 10 min DNase treatment and 30 min post-transcriptional polyadenylation using a Poly(A) Tailing Kit (Thermo Fisher Scientific). saRNA was purified using a MEGAclear Transcription Clean-Up Kit (Thermo Fisher Scientific) and eluted in DNase-free and RNase-free water before storing at –80 °C. The absorbance at a wavelength of 260 nm of an equimolar, 1 mM mixture of all combinations of modified NTPs and NTPs was empirically determined using a NanoDrop2000 (Thermo Fisher Scientific). The adjusted factor for each modified NTP was used to calculate RNA concentration to ensure consistent delivery of modified NTPs (Table 1). RNA quality was assessed by denaturing gel electrophoresis. To measure dsRNA content, RNA (40–1,000 ng) was blotted onto Whatman Nytran Super-Charge membranes (Cytiva), blocked with 5% nonfat dried milk in PBS-T buffer and then incubated overnight at 4 °C with dsRNA (76651, Cell Signaling Technologies) antibody at a 1:1,000 dilution or DNA–RNA hybrid antibody (S9.6, Active Motif) at a 1:5,000 dilution. Poly(I:C) (InVivoGen) was used as a positive control. The membranes were washed five times with PBS-T before incubation with horseradish peroxidase (HRP)-conjugated goat anti-mouse IgG secondary antibodies (1030-05, Southern Biotech) at a 1:10,000 dilution. The membranes were washed another five times with PBS-T and incubated for 5 min with SuperSignal West Pico PLUS Chemiluminescent Substrate (Thermo Fisher Scientific). Images were captured with an iBright Imaging System (Thermo Fisher Scientific).

Modified NTP saRNA screening in HEK293T

HEK293T cells were grown in DMEM containing 1 mM sodium pyruvate, 10% FBS and 1% penicillin–streptomycin, plated at 70,000 cells per cm² in 96-well plates and allowed to adhere overnight. For the modified NTP screen, mCherry saRNA was transfected using Lipofectamine MessengerMax Transfection Reagent, according to the manufacturer's protocol (Thermo Fisher Scientific). Twenty-four hours later, cells were prepared for flow cytometry analysis of mCherry expression.

Cells were washed with 1X PBS, treated with 1X PBS containing 2 mM EDTA for 5 min and resuspended in fluorescence-activated cell sorting buffer (1X PBS with 2% BSA). Data were acquired using the Attune NxT Flow Cytometer (Thermo Fisher Scientific) and analyzed using FlowJo (v10.8.1). Fluorescence microscopy of selected modified NTPs was performed on a BioTek Cytation 5 microscope before preparation for flow cytometry analysis.

LNP formulation

saRNAs were encapsulated within LNPs with the following composition (mole percent): 50% SM-102 (33474, Cayman), 1.5% DMG-PEG 2000 (880151, Avanti Polar Lipids), 10% 18:1 (Δ9-Cis) PE (DOPE) (850725, Avanti Polar Lipids) and 38.5% cholesterol (700100, Avanti Polar Lipids). RNA was loaded at an N:P molar ratio of 10. Before formulation, the aqueous and lipid phases were sterile filtered separately through 0.22-μm filters. Formulations were performed in sterile RNase-free conditions. After formulation, the LNPs were dialyzed against sterile RNase free 1X PBS for 24 h at 4 °C. LNP morphology was characterized by dynamic light scattering using a NanoBrook Omni (Brookhaven Instruments). Encapsulation efficiency was determined using the QuantiFluor RNA System (Promega). To transfect primary T cells, monoclonal antibody-targeted LNPs were formulated using the post-insertion method⁵⁵ with 0.1 mol% DSPE-PEG(2000) Maleimide (880126, Avanti Polar Lipids) for 1 h at room temperature. Next, the LNPs were reacted for 1 h at room temperature with anti-CD3, which was reduced with 1 mM tris(2-carboxyethyl)phosphine for 1 h at room temperature (clone OKT3, BioXCell).

Expression potentiation assays

HEK293T and C2C12 cells were grown in DMEM containing 10% FBS and 1% penicillin–streptomycin, and were passaged every 3 days. Twenty-four hours before transfection, the cells were washed with PBS, trypsinized and plated in 200 μl DMEM at 50,000 cells per well for HEK293T cells and 25,000 cells per well for C2C12 cells. For transfection, LNPs containing mRNA or saRNA encoding luciferase were added dropwise to the cells in triplicate at 10 ng or 100 ng per well. After 24 h, the luciferase expression was assayed using the Bright-Glo Luciferase Assay System (Promega).

Jurkat cells were grown in RPMI containing 10% FBS and 1% penicillin–streptomycin and were maintained between 5×10^5 and 1×10^6 cells per ml. Before transfection, the cells were washed with PBS and plated in 200 μl RPMI at 250,000 cells per well. For transfection, LNPs containing saRNA with or without modified nucleotides were added dropwise to cells in triplicate at 25, 100 or 250 ng per well. After 24 h, some cells were collected for flow cytometry analysis. The remainder of the cells were maintained in culture and assayed using flow cytometry at additional time points. For electroporation, Jurkat cells were washed three times with OptiMEM, and one million cells were electroporated with 1 μg of saRNA in OptiMEM buffer using a 4D-Nucleofector System (Lonza).

Primary human CD3⁺ T cells from three unique donors were isolated by negative selection (RosetteSep T Cell Enrichment Cocktail, STEMCELL Technologies) from peripheral blood and were grown in RPMI containing 10% FBS and 1% penicillin–streptomycin supplemented with 50 U ml⁻¹ interleukin (IL)-2, 10 ng ml⁻¹ IL-7 and 10 ng ml⁻¹ IL-15. To activate the cells, Dynabeads Human T-Activator CD3/CD28 (Thermo Fisher Scientific) were added to the cells at a 1:1 bead-to-cell ratio and incubated for 24 h. After activation, the Dynabeads were removed, and the T cells were rested for 24 h before transfection. Primary T cells were washed with PBS and plated at 100,000 cells per well in RPMI containing 10% FBS and 50 U ml⁻¹ IL-2. For transfection, anti-CD3-conjugated LNPs (500 ng/dose) were dosed to each of three wells (for n = 3 biological replicates) such that the final volume in each well was 200 μl.

Primary human foreskin fibroblasts were grown in EMEM containing 10% FBS and 1% penicillin–streptomycin, washed with PBS

and plated at 10,000 cells per well in DMEM containing 10% FBS. For transfection, LNPs were dosed in triplicate at different doses such that the final volume in each well was 200 μ l.

PBMC early IFN response

Human PBMCs were thawed and rested for 24 h in RPMI containing 10% FBS and 1% penicillin–streptomycin. A total of 500,000 cells (one million cells per milliliter) were plated in wells of a 24-well plate, and 250 ng of saRNA encapsulated within LNPs, formulated as previously described, was added dropwise to the PBMCs. After 6 or 24 h, the medium was collected after centrifugation and analyzed for IFN expression using the Human IFN- α All Subtype Quantikine ELISA Kit (R&D Systems) and the Human IFN- β DuoSet ELISA (R&D Systems). cDNA was generated using the High-Capacity cDNA Reverse Transcription Kit (Thermo Fisher Scientific), according to the manufacturer's protocol. qPCR for specific genes was carried out using TaqMan probes in TaqMan Fast Advanced Master Mix (Thermo Fisher Scientific). A Ubiquitin C probe with 2'-chloro-7'-phenyl-1,4-dichloro-6-carboxyfluorescein (VIC) dye was used as the endogenous control for all qPCRs.

Antigen production in C2C12 Cells

C2C12 cells were grown in DMEM containing 10% FBS and 1% penicillin–streptomycin, plated at 25,000 cells per well in 96-well tissue culture-treated plates and allowed to adhere overnight. For transfection, LNPs containing mRNA or saRNA encoding each antigen were added to cells in triplicate at 100 ng per well, except for hemagglutinin-encoding RNAs, which were dosed at 25 ng per well. After 24 h, cells were collected for flow cytometry analysis using the following monoclonal antibodies: SARS-CoV-2 Spike Protein (RBD) Human Monoclonal Antibody (51-6490-82, Thermo Fisher Scientific, 1:100 dilution) and Influenza A H1N1 (A/California/07/2009) Hemagglutinin/HA Antibody (11085-T62, SinoBiological, 1:1,000 dilution, APC conjugated). Identical treatments were performed for ELISA confirmation. Cells for ELISA were washed twice with PBS and then resuspended in 1X PBS containing 0.1% Triton X-100. Cells underwent one freeze–thaw cycle before thorough mixing with a pipette to ensure lysis and membrane disruption. ELISA was performed with antigen-specific sandwich ELISA kits according to the manufacturer's protocol (SinoBiological).

Institutional approvals

All animal experiments described in this study were performed in accordance with protocols that were reviewed and approved by the Institutional Animal Care and Use Committee of Boston University (PROTO202100000026, PROTO202000020 and PROTO201800600). All mice were maintained in facilities accredited by the Association for the Assessment and Accreditation of Laboratory Animal Care. Vaccination studies and replication-competent SARS-CoV-2 experiments were performed in biosafety level 2 (BSL-2) and biosafety level 3 (BSL-3) laboratories, respectively, at the Boston University National Emerging Infectious Diseases Laboratories (NEIDL). Bioluminescent imaging experiments were performed at Boston University.

Bioluminescent imaging

Female C57BL/6J mice 6–8 weeks old were obtained from The Jackson Laboratory (000664) and group housed in a room with lights maintained on a 12-h light/dark cycle, a temperature range of 20–26 $^{\circ}$ C, and 30–70% humidity. Mice were administered 50 μ l of PBS or LNPs containing 2.5 μ g of mRNA or saRNA by i.m. injections in the left hind limb. For imaging, the mice were anesthetized with 1–2% isoflurane and administered IVISbrite D-Luciferin Rediject Solution (PerkinElmer) by intraperitoneal injections 10 min before imaging. Imaging was performed with an IVIS Spectrum (PerkinElmer). Total flux analysis was performed with Aura Imaging Software (Spectral Instruments Imaging).

Virus production cell culture

VeroE6 cells were grown in DMEM (Thermo Fisher Scientific) supplemented with 10% heat-inactivated FBS (Bio-Techne) and 1% penicillin–streptomycin (Thermo Fisher Scientific). A549-hACE2-TMPRSS2 cells were maintained in DMEM containing 10% FBS, 1% penicillin–streptomycin and 2.5 μ g ml⁻¹ puromycin and blasticidin. All cell lines were maintained in a cell incubator at 37 $^{\circ}$ C with 5% CO₂.

SARS-CoV-2 isolate stock

All replication-competent SARS-CoV-2 experiments were performed in a BSL-3 facility at the Boston University NEIDL. SARS-CoV-2 MA30 was a generous gift of S. Perlman (University of Iowa), and rSARS-CoV-2 WA-1/mNeonGreen was a generous gift of P.-Y. Shi (University of Texas Medical Branch). Viral stocks were prepared and titered as previously described⁵⁶.

Mouse vaccine studies

Male and female C57BL/6J mice 8–10 weeks old were obtained from The Jackson Laboratory (000664). In the NEIDL BSL-2 and BSL-3 facilities, mice were group housed by sex in Green Line individually ventilated cages (Tecniplast). The room was maintained with a 12-h light/dark cycle at 20–26 $^{\circ}$ C and 30–70% humidity. Mice were administered 50 μ l of PBS or LNPs containing 10 ng, 100 ng or 1,000 ng of mRNA or saRNA by i.m. injections in the hind limb. At 24 h and 48 h post vaccination, serum was collected by submandibular bleeding from five mice from each of the groups that received 1,000 ng mRNA or saRNA vaccinations for an analysis of the IFN response. At 21 days post initial vaccination, mice were administered a booster dose of PBS or vaccine (50 μ l i.m., a dosage similar to that of the primary vaccination). At 35 days post vaccination, mice were transferred to the BSL-3 facility and challenged with MA30 virus, as described below.

SARS-CoV-2 challenge experiments

Vaccinated and boosted mice were intranasally inoculated with 1×10^5 plaque-forming units of SARS-CoV-2 MA30 virus resuspended in 50 μ l of 1X PBS. Mice were inoculated under 1–3% isoflurane anesthesia. Infected mice were monitored and clinically scored for changes in weight, respiration, appearance, responsiveness and behavior for 14 days post infection. Mice with a cumulative clinical score of 4, or greater than 20% weight loss, were euthanized.

Serum preparation

Blood was collected at the designated time points by submandibular bleeding, and serum was isolated by centrifuging blood in a benchtop centrifuge at 1,000g for 10 min at room temperature. Serum was then collected, transferred to a new Eppendorf tube and stored at –80 $^{\circ}$ C for downstream analysis.

Serum IFN analysis

Serum IFN α 1 and IFN β were analyzed using the ELISA MAX Deluxe Set Mouse IFN- α 1 (447904, BioLegend) and the LEGEND MAX Mouse IFN- β ELISA Kit (439407, BioLegend), respectively.

SARS-CoV-2 spike IgG titer measurements

Total SARS-CoV-2 spike binding IgG antibody titers were measured using ELISA. Nunc Maxisorp ELISA Plates (96 wells, 423501, BioLegend) were coated overnight at 4 $^{\circ}$ C with 0.5 μ g ml⁻¹ of recombinant SARS-CoV-2 Spike His Protein (10549-CV, R&D Systems) in PBS. The plates were blocked with 1% BSA in PBS. Binding IgG was detected using HRP-conjugated Goat Anti-Mouse IgG (1030-05, Southern Biotech). A dilution series of purified SARS-CoV-2 neutralizing monoclonal antibodies was used for standardized quantification (A02057, Genscript). TMB Substrate Solution (N301, Thermo Fisher Scientific) with sulfuric acid stop solution was used for colorimetric detection.

Serum neutralization assay

The day before experiments, 2×10^4 A549-hACE2-TMPRSS2 cells were plated in 96-well plates. Decomplementation of serum was performed at 56 °C for 30 min. Serum was diluted 1:5 in OptiMEM, and subsequent threefold dilutions were prepared. Diluted serum was mixed with rSARS-CoV-2 WA-1/mNeonGreen (2019-nCoV/USA-WA1/2020 strain) for 1 h at room temperature before plating. Viral adsorption was performed at 37 °C for 1 h. The serum–virus mixture was removed, and 200 μ l of fresh DMEM containing 2% FBS and 1% penicillin–streptomycin was added to each well. Cells were then incubated for 24 h at 37 °C with 5% CO₂. After incubation, cells were trypsinized, washed with 1X PBS and fixed with 4% paraformaldehyde for 1 h. Cells were analyzed on a Beckman Coulter LSRII Flow Cytometer and analyzed using FlowJo analysis software (v10.9.0).

Statistical analysis

All statistical analyses were performed using GraphPad Prism 9. Each statistical test was performed as described in the figure legends.

Reporting summary

Further information on research design is available in the Nature Portfolio Reporting Summary linked to this article.

Data availability

Antigen sequences used in the current study are accessible from NCBI. The NCBI reference sequence for the influenza A hemagglutinin (Influenza A virus (A/California/07/2009(H1N1))) is available at [YP_009118626.1](https://www.ncbi.nlm.nih.gov/nuclot/YP_009118626.1), and the NCBI reference sequence for the SARS-CoV-2 spike protein with K986P-stabilizing and V987P-stabilizing mutations (Wuhan-Hu-1) is available at [YP_009724390.1](https://www.ncbi.nlm.nih.gov/nuclot/YP_009724390.1). The source data supporting the findings of the study are available with the manuscript as a supplementary file.

References

53. Petrakova, O. et al. Noncytopathic replication of Venezuelan equine encephalitis virus and eastern equine encephalitis virus replicons in mammalian cells. *J. Virol.* **79**, 7597–7608 (2005).
54. Yoshioka, N. et al. Efficient generation of human iPSCs by a synthetic self-replicative RNA. *Cell Stem Cell* **13**, 246–254 (2013).
55. Swart, L. E. et al. A robust post-insertion method for the preparation of targeted siRNA LNPs. *Int. J. Pharm.* **620**, 121741 (2022).
56. Kenney, D. J. et al. Humanized mice reveal a macrophage-enriched gene signature defining human lung tissue protection during SARS-CoV-2 infection. *Cell Rep.* **39**, 110714 (2022).

Acknowledgements

W.W.W. acknowledges support from the National Institutes of Health (NIH) (U01CA265713, R01EBO29483, R01DK132576 and R01EBO31904). M.W.G. acknowledges support from the NIH (U01CA265713) and the William Fairfield Warren Professorship. F.D. acknowledges

support from a Boston University startup fund, a Peter Paul Career Development Professorship and a National Institute of Allergy and Infectious Diseases K22 transition award (K22AI144050). D.K. acknowledges support from the NIH T32 Immunology Training Program (T32AI007309). We thank the IVIS Imaging Core Facility (1S1ORR024523-01), the NEIDL animal core and the NEIDL operations staff for their outstanding support. T.S. acknowledges support from a Lung Cancer Research Fellowship. J.E.M. acknowledges support from the National Science Foundation (NSF) Graduate Research Fellowship Program (GRFP). J.E.M. and J.R.K. were supported by the NIH T32 Translational Research in Biomaterials Training Program (T32EB006359). This material is based upon work supported by the NSF GRFP (2234657). Any opinions, findings and conclusions or recommendations expressed in this material are those of the authors and do not necessarily reflect the views of the NSF. This research was supported in part by an NIH training grant at Boston University (T32EB006359). The content is solely the responsibility of the authors and does not necessarily represent the official views of the NIH. Fig. 2 was partially generated with [BioRender.com](https://www.biorender.com). Source data are provided with this paper.

Author contributions

J.E.M., J.R.K., M.W.G. and W.W.W. conceptualized the study. J.E.M. and J.R.K. designed and assembled RNA constructs and conducted in vitro experiments. D.K. and E.C.C. performed in vivo experiments involving the SARS-CoV-2 vaccine. F.C. performed studies characterizing vaccine immunogenicity. T.-Y.S. and J.E.M. performed in vivo bioluminescent imaging. J.E.M., J.R.K., M.W.G., W.W.W. and F.D. were involved in study design. All authors provided feedback and contributed to manuscript preparation.

Competing interests

W.W.W. holds equity in Senti Biosciences, 4Immune Therapeutics and Keylicon Biosciences. A patent has been filed based on the findings of this work (J.E.M., W.W.W., M.W.G. and J.R.K.). J.E.M., M.W.G. and J.R.K. hold equity in Keylicon Biosciences. All other authors have no competing interests.

Additional information

Supplementary information The online version contains supplementary material available at <https://doi.org/10.1038/s41587-024-02306-z>.

Correspondence and requests for materials should be addressed to Florian Douam, Wilson W. Wong or Mark W. Grinstaff.

Peer review information *Nature Biotechnology* thanks Corey Casper and the other, anonymous, reviewer(s) for their contribution to the peer review of this work.

Reprints and permissions information is available at www.nature.com/reprints.

Reporting Summary

Nature Portfolio wishes to improve the reproducibility of the work that we publish. This form provides structure for consistency and transparency in reporting. For further information on Nature Portfolio policies, see our [Editorial Policies](#) and the [Editorial Policy Checklist](#).

Statistics

For all statistical analyses, confirm that the following items are present in the figure legend, table legend, main text, or Methods section.

n/a Confirmed

- The exact sample size (n) for each experimental group/condition, given as a discrete number and unit of measurement
- A statement on whether measurements were taken from distinct samples or whether the same sample was measured repeatedly
- The statistical test(s) used AND whether they are one- or two-sided
Only common tests should be described solely by name; describe more complex techniques in the Methods section.
- A description of all covariates tested
- A description of any assumptions or corrections, such as tests of normality and adjustment for multiple comparisons
- A full description of the statistical parameters including central tendency (e.g. means) or other basic estimates (e.g. regression coefficient) AND variation (e.g. standard deviation) or associated estimates of uncertainty (e.g. confidence intervals)
- For null hypothesis testing, the test statistic (e.g. F , t , r) with confidence intervals, effect sizes, degrees of freedom and P value noted
Give P values as exact values whenever suitable.
- For Bayesian analysis, information on the choice of priors and Markov chain Monte Carlo settings
- For hierarchical and complex designs, identification of the appropriate level for tests and full reporting of outcomes
- Estimates of effect sizes (e.g. Cohen's d , Pearson's r), indicating how they were calculated

Our web collection on [statistics for biologists](#) contains articles on many of the points above.

Software and code

Policy information about [availability of computer code](#)

Data collection

Data analysis

For manuscripts utilizing custom algorithms or software that are central to the research but not yet described in published literature, software must be made available to editors and reviewers. We strongly encourage code deposition in a community repository (e.g. GitHub). See the Nature Portfolio [guidelines for submitting code & software](#) for further information.

Data

Policy information about [availability of data](#)

All manuscripts must include a [data availability statement](#). This statement should provide the following information, where applicable:

- Accession codes, unique identifiers, or web links for publicly available datasets
- A description of any restrictions on data availability
- For clinical datasets or third party data, please ensure that the statement adheres to our [policy](#)

Antigen sequences utilized in the current study are accessible from NCBI: Influenza A Hemagglutinin (Influenza A virus (A/California/07/2009(H1N1)), NCBI Ref Seq: YP_009118626.1), SARS-CoV-2 Spike (Wuhan-Hu-1, NCBI Ref Seq: YP_009724390.1) with K986P and V987P stabilizing mutations. The source data supporting the findings of the study are available with the manuscript as a supplementary file.

Research involving human participants, their data, or biological material

Policy information about studies with [human participants or human data](#). See also policy information about [sex, gender \(identity/presentation\), and sexual orientation](#) and [race, ethnicity and racism](#).

Reporting on sex and gender	Information about the sex or gender was not provided for human donors.
Reporting on race, ethnicity, or other socially relevant groupings	Information about the race, ethnicity, or socially relevant groupings were not provided for human donors.
Population characteristics	Information about the population characteristics were not provided for human donors.
Recruitment	Information about the recruitment for sample collection was not provided.
Ethics oversight	All protocols were approved by the Institutional Biosafety Committee (IBC).

Note that full information on the approval of the study protocol must also be provided in the manuscript.

Field-specific reporting

Please select the one below that is the best fit for your research. If you are not sure, read the appropriate sections before making your selection.

Life sciences Behavioural & social sciences Ecological, evolutionary & environmental sciences

For a reference copy of the document with all sections, see nature.com/documents/nr-reporting-summary-flat.pdf

Life sciences study design

All studies must disclose on these points even when the disclosure is negative.

Sample size	For all in vitro assays, sample size is the number of wells receiving each treatment condition. No statistical methods were utilized to predetermine sample sizes. All in vitro experiments were performed with an n = 3 or greater. This sample size has been shown to be sufficient to ensure reproducibility in our previous studies. For all in vivo data, each group contains an n of at least 5 (5 distinct mice receiving each treatment). This sample size has been shown to be sufficient to ensure reproducibility in our previous studies.
Data exclusions	In figure 2, mice that were infected with live virus and were monitored and clinically scored for changes in weight, respiration, appearance, responsiveness and behavior over the course of 14-days post infection. Mice with a cumulative clinical score of 4 or 20% weight loss were euthanized. In figure 2B, one mouse was excluded from the m5C saRNA group on day 10 due to experimenter error with substrate injection.
Replication	A majority of the in vitro assays were performed with multiple cell lines and multiple times to confirm reproducibility. Hits identified in the screen from Figure 1C were reproduced by transfection of additional batches of RNA from distinct in vitro transcription reactions. Transfections performed in Figure 1 were performed multiple times and with multiple cell lines to confirm reproducibility. For the primary T transfection assay in Figure 1H, 3 distinct human PBMC donors were utilized in the assays to account for donor variability. For the immunogenicity assays in Figure 1, 3 distinct human PBMC donors were utilized in the assays to account for donor variability. For transfection of cells to express viral antigens in Figure 2, transfections were performed multiple times in multiple cell lines. For the bioluminescent imaging in Figure 2, an n = 5 per group was utilized to assay variability in each group. For the vaccination and protection study in Figure 2 an n = 10-20 was utilized for each group with 5 to 10 male and 5 to 10 female mice. Gel analysis was conducted at least two times with different batches of RNA. All replication attempts resulted in similar findings as original experiments.
Randomization	For the vaccination study, 5 to 10 male and 5 to 10 female mice were randomly assigned to receive a dose of either PBS, N1-methylpseudouridine mRNA, WT self-amplifying RNA, or 5mC self-amplifying RNA at 10 ng, 100 ng, or 1000 ng. For the in vivo luciferase experiment, mice were randomly assigned to groups. For all in vitro assays, experimental groups were determined randomly by assigning plate layouts after addition of cells to respective well plates.
Blinding	Experimenters performing vaccination experiments with mice were blinded to treatment conditions when possible. For imaging of the mice in the luciferase study, experimenters were not blinded to the identity of the mice. For all in vitro experiments, experimenters were not blinded to the identity of the samples being analyzed.

Reporting for specific materials, systems and methods

We require information from authors about some types of materials, experimental systems and methods used in many studies. Here, indicate whether each material, system or method listed is relevant to your study. If you are not sure if a list item applies to your research, read the appropriate section before selecting a response.

Materials & experimental systems

Methods

n/a	Involved in the study
<input type="checkbox"/>	<input checked="" type="checkbox"/> Antibodies
<input type="checkbox"/>	<input checked="" type="checkbox"/> Eukaryotic cell lines
<input checked="" type="checkbox"/>	<input type="checkbox"/> Palaeontology and archaeology
<input type="checkbox"/>	<input checked="" type="checkbox"/> Animals and other organisms
<input checked="" type="checkbox"/>	<input type="checkbox"/> Clinical data
<input checked="" type="checkbox"/>	<input type="checkbox"/> Dual use research of concern
<input checked="" type="checkbox"/>	<input type="checkbox"/> Plants

n/a	Involved in the study
<input checked="" type="checkbox"/>	<input type="checkbox"/> ChIP-seq
<input type="checkbox"/>	<input checked="" type="checkbox"/> Flow cytometry
<input checked="" type="checkbox"/>	<input type="checkbox"/> MRI-based neuroimaging

Antibodies

Antibodies used

Flow antibodies:

SARS-CoV-2 Spike Protein (RBD) Human monoclonal (eBiosciences - Clone: P05Dhu – AF647 conjugated), (1:100 dilution)
Influenza A H1N1 (A/California/07/2009) Hemagglutinin, Rabbit polyclonal: (1:1000 dilution) (SinoBiological - Cat: 11085-T62 – APC conjugated)

ELISA antibodies:

Human IFN-alpha All Subtype Quantikine ELISA - R&D Systems
Human IFN-beta DuoSet ELISA R&D Systems
LEGEND MAX™ Mouse IFN-β ELISA Kit – BioLegend
ELISA MAX™ Deluxe Set Mouse IFN-α1 – BioLegend
HRP conjugated goat anti-mouse IgG secondary (Southern Biotech, 1030-05)

Dotblot antibodies:

dsRNA (J2) Mouse mAb - Cell Signaling Technology #76651
DNA-RNA Hybrid antibody (S9.6) Mouse mAb (Active Motif, 65684)
HRP conjugated goat anti-mouse IgG secondary (Southern Biotech, 1030-05)

Targeted LNPs:

InVivoMab anti-human CD3 (BioXCell, Clone OKT3, BE0001-2)

Validation

SARS-CoV-2 Spike Protein (RBD) Human monoclonal validated: "This P05Dhu Alexa Fluor™ 647 conjugate has been tested by flow cytometric analysis of HEK 293 cells transfected with a vector encoding full length spike protein from SARS CoV2."

Influenza A H1N1 (A/California/07/2009) Hemagglutinin, Rabbit polyclonal validated by Western Blot and ELISA according to manufacturer.

Human IFN-alpha All Subtype Quantikine ELISA - R&D Systems validated against natural and recombinant human IFN-alpha according to supplier.

Human IFN-beta DuoSet ELISA R&D Systems validated against natural and recombinant human IFN-beta according to supplier.

LEGEND MAX™ Mouse IFN-β ELISA Kit – BioLegend has verified reactivity against mouse IFN-beta according to supplier.

ELISA MAX™ Deluxe Set Mouse IFN-α1 – BioLegend has verified activity against mouse IFN-alpha1 according to supplier.

dsRNA (J2) Mouse mAb - Cell Signaling Technology #76651 validated by "IF staining and analysis of Vero cells infected with SARS-CoV-2" according to supplier.

DNA-RNA Hybrid antibody (S9.6) Mouse mAb (Active Motif, 65684) validated by dotblot according to supplier.

InVivoMab anti-human CD3 (BioXCell, Clone OKT3, BE0001-2) is well described for various T cell applications described in references:

Wunderlich, M., et al. (2014). "OKT3 prevents xenogeneic GVHD and allows reliable xenograft initiation from unfractionated human hematopoietic tissues" *Blood* 123(24): e134-144.

Lines, J. L., et al. (2014). "VISTA is an immune checkpoint molecule for human T cells" *Cancer Res* 74(7): 1924-1932.

Esposito, L., et al. (2014). "Investigation of soluble and transmembrane CTLA-4 isoforms in serum and microvesicles" *J Immunol* 193(2): 889-900.

Eukaryotic cell lines

Policy information about [cell lines and Sex and Gender in Research](#)

Cell line source(s)

All cell lines were sourced from ATCC and were maintained below passage 20.
Cell lines utilized in the study include: HEK293T, Jurkat, C2C12, HFF-1

Authentication

None of the cell lines were authenticated after receiving from ATCC. Morphologies of each cell line were consistent with expected morphologies.

Mycoplasma contamination	All cell lines were routinely tested for mycoplasma and none were identified as being contaminated at any point of the study.
Commonly misidentified lines (See ICLAC register)	HEK293T were used for modNTP screen and transfection assays in Figure 1 and Figure S2.

Animals and other research organisms

Policy information about [studies involving animals](#); [ARRIVE guidelines](#) recommended for reporting animal research, and [Sex and Gender in Research](#)

Laboratory animals	8-10 weeks old male and female C57BL/6J mice were obtained from Jackson Laboratories (Bar Harbor, ME, USA, Catalog # 000664) for the vaccine studies. In the NEIDL BSL-2 and -3 facility, mice were group-housed by sex in Techniplast green line individually ventilated cages (Techniplast, Buguggiate, Italy). The room was maintained with a 12:12 light cycle at 68-79°F and 30-70% humidity. 6-8 weeks old female C57BL/6J mice were obtained from Jackson Laboratories (Bar Harbor, ME, USA, Catalog # 000664) for the luciferase study. For the luciferase study, mice were group-housed. The room was maintained with a 12:12 light cycle at 68-79°F and 30-70% humidity.
Wild animals	This study did not involve wild animals.
Reporting on sex	For the luciferase BLI imaging studies, all animals were female. For the vaccination study, 5 to 10 male and 5 to 10 female mice were included in each group.
Field-collected samples	No field collected samples were involved in this study.
Ethics oversight	All animal experiments described in this study were performed in accordance with protocols that were reviewed and approved by the Institutional Animal Care and Use and Committee of Boston University (PROTO20210000026, PROTO202000020, and PROTO201800600). All mice were maintained in facilities accredited by the Association for the Assessment and Accreditation of Laboratory Animal Care (AAALAC). Vaccination studies and replication-competent SARS-CoV-2 experiments were performed in a biosafety level 2 and 3 laboratory (BSL-3), respectively at the Boston University National Emerging Infectious Diseases Laboratories (NEIDL). Bioluminescent imaging experiments were performed at Boston University.

Note that full information on the approval of the study protocol must also be provided in the manuscript.

Flow Cytometry

Plots

Confirm that:

- The axis labels state the marker and fluorochrome used (e.g. CD4-FITC).
- The axis scales are clearly visible. Include numbers along axes only for bottom left plot of group (a 'group' is an analysis of identical markers).
- All plots are contour plots with outliers or pseudocolor plots.
- A numerical value for number of cells or percentage (with statistics) is provided.

Methodology

Sample preparation	Cells were prepared for flow cytometry analysis in a live state, directly from cell culture. Adherent cells were washed 2x with PBS, detached with EDTA and gentle trypsinization (0.05%), and washed and resuspended in PBS + 2% BSA prior to analysis. Suspension cells were washed 2X with PBS, and resuspended in PBS + 2% BSA. Cells were stained with fluorescent antibodies for 1 hour at 4C in a dark environment. For serum neutralization experiment the cells were trypsinized, washed with 1X PBS, and fix with 4% paraformaldehyde (PFA) for one hour. Cells were acquired on a Beckman Coulter LSRII Flow cytometer and analyzed using FlowJo analysis software.
Instrument	ThermoFisher Scientific Attune NxT Flow Cytometer, Beckman Coulter LSRII
Software	FlowJo v10
Cell population abundance	Cells were analyzed directly with >10,000 events reported for all reported samples.
Gating strategy	Gating strategy is summarized as a supplementary figure. Oval gates were used to isolate cells from dead cells/debris using SSC-A vs FSC-A. Singlets were gated using FSCH-H and FSC-A. For cells expected to express a fluorescent protein, gating was performed from untreated/untransfected cells. For surface staining of viral antigens, an unstained condition was utilized as well as an untreated but stained condition. Gating was performed off of the untreated + stained condition.

- Tick this box to confirm that a figure exemplifying the gating strategy is provided in the Supplementary Information.